

# Primordial nucleosynthesis with varying fundamental constants

## Solutions to the lithium problem and the deuterium discrepancy

M. Deal<sup>1,2</sup>  and C. J. A. P. Martins<sup>1,2</sup> 

<sup>1</sup> Centro de Astrofísica da Universidade do Porto, Rua das Estrelas, 4150-762 Porto, Portugal  
e-mail: [Morgan.Deal@astro.up.pt](mailto:Morgan.Deal@astro.up.pt), [Carlos.Martins@astro.up.pt](mailto:Carlos.Martins@astro.up.pt)

<sup>2</sup> Instituto de Astrofísica e Ciências do Espaço, CAUP, Rua das Estrelas, 4150-762 Porto, Portugal

Received 4 March 2021 / Accepted 24 June 2021

### ABSTRACT

The success of primordial nucleosynthesis has been limited by the long-standing lithium problem. We use a self-consistent perturbative analysis of the effects of the relevant theoretical parameters on primordial nucleosynthesis, including variations of nature's fundamental constants, to explore the problem and its possible solutions in the context of the latest observations and theoretical modeling. We quantify the amount of depletion needed to solve the lithium problem, and show that transport processes of chemical elements in stars are able to account for it. Specifically, the combination of atomic diffusion, rotation, and penetrative convection allows us to reproduce the lithium surface abundances of Population II stars, starting from the primordial lithium abundance. We also show that even with this depletion factor, a preference for a value of the fine-structure constant at this epoch remains that is larger than the value currently obtained in the laboratory by a few parts per million of relative variation at a statistical significance level of two to three standard deviations. This preference is driven by the recently reported discrepancy between the best-fit values for the baryon-to-photon ratio (or equivalently, the Deuterium abundance) inferred from cosmic microwave background and primordial nucleosynthesis analyses, and is largely insensitive to the Helium-4 abundance. We thus conclude that the lithium problem most likely has an astrophysical solution, while the Deuterium discrepancy provides a possible indication of new physics.

**Key words.** nuclear reactions, nucleosynthesis, abundances – primordial nucleosynthesis – stars: abundances – stars: evolution – cosmology: theory – methods: statistical

## 1. Introduction

Big Bang nucleosynthesis (henceforth BBN) is a cornerstone of the standard particle cosmology paradigm and a sensitive probe of physics beyond the standard model (Steigman 2007; Iocco et al. 2009; Pitrou et al. 2018). Nevertheless, its success is limited by the well-known lithium problem, which describes the excess of the theoretically expected abundance of lithium-7 (given our present knowledge of astrophysics, nuclear and particle physics) to the observed abundance of a factor of about 3.5 (Zyla et al. 2020). Although many attempts have been made to solve the problem, there is no clear known solution. Further discussion of these solutions can be found in Fields (2011), Mathews et al. (2020), and the BBN section of the latest Particle Data Group (henceforth PDG), review by Zyla et al. (2020).

Recent progress in experimental measurements of the required nuclear cross-sections has all but excluded the possibility of nuclear physics systematics (Iliadis & Coc 2020; Mossa et al. 2020). On the astrophysics side, some degree of lithium depletion can occur in stars due to the mixing of the outer layers with the hotter interior (Sbordone et al. 2010), and some authors have suggested that a depletion by factor as large as 1.8 may have occurred (Ryan et al. 2000; Korn et al. 2006). It has been argued that this scenario might be difficult to reconcile with the existence of extremely iron-poor dwarf stars with lithium abundances very close to the Spite plateau (Aguado et al. 2019), but there is no consensus on this point. Finally, the lithium

problem could also point to new physics beyond the standard model; one such possibility is the variation of nature's fundamental constants, which is unavoidable in many extensions of the standard particle physics and cosmological models (Damour et al. 2002); a recent review of the topic is Martins (2017). This possibility has recently been revisited in Clara & Martins (2020) and Martins (2021) (henceforth Paper 1 and Paper 2, respectively), who showed that there is a preference for a value of the fine-structure constant,  $\alpha$ , at the BBN epoch that is higher than the current laboratory constant by a few parts per million of relative variation, even when allowing for possible changes to the most relevant cosmological parameters impacting BBN: the neutron lifetime, the number of neutrino species, and the baryon-to-photon ratio.

Stars are formed with an initial chemical composition representative of their birth environment. During their evolution, this chemical composition is modified by several processes, namely nuclear reactions and transport processes. Nuclear reactions affect the abundance profiles of some elements in the central region of stars, increasing or decreasing their abundances. Transport processes of chemical elements modify the element distribution in the whole star. There are macroscopic transport processes such as convection, which efficiently transports chemical elements and leads to an homogenized chemical composition in the convective zone. Other macroscopic transport processes are less efficient and reduce the potential internal gradient of the chemical composition while transporting

them deeper into the stars (i.e., transport induced by rotation; e.g., Palacios et al. 2003; Talon 2008; Maeder 2009, and references therein; and thermohaline convection; e.g., Vauclair 2004; Denissenkov 2010; Brown et al. 2013; Deal et al. 2016, and references therein). These macroscopic transport processes compete with microscopic transport processes, namely atomic diffusion (see Michaud et al. 2015, for a detailed description). This comes from physics first principles and is induced by the internal gradients of pressure, temperature, and composition. It is efficient in radiative zones and leads to a selective transport of chemical elements, mainly driven by the competition between the gravity and radiative accelerations. Gravity moves elements toward the center of stars, while radiative accelerations, a mechanism for transfer of momentum between photons and ions, move some elements toward the surface of stars (depending on their ionization states and abundances). As a consequence, the surface abundance of elements are either higher or lower than the initial elemental abundances. Considering all the potential processes affecting the chemical elements distribution in stars, it is expected that the observed surface abundances are often different from the initial abundances, especially on the main sequence, where the surface convective zones are not too deep to allow surface abundance variations.

Light elements (such as lithium and beryllium) are especially affected by transport processes during the evolution of stars. Atomic diffusion leads to a depletion of these elements from the surface (radiative accelerations are negligible for these elements most of the time). Moreover, these elements are destroyed by nuclear reactions at rather low temperatures (about 2.5 and 3.5 million K for lithium and beryllium, respectively) not very deep inside stars. When macroscopic transport processes are efficient enough and affect deep regions, lithium is then transported in regions where the temperature is high enough for it to be destroyed by nuclear reactions. The combination of atomic diffusion and macroscopic transport processes is expected to lead to a discernible depletion of lithium from the surface, hence to lithium-7 surface abundances that are lower than the initial abundance (e.g., Vauclair 1988; Charbonnel et al. 1994; Korn et al. 2006, 2007; Gruyters et al. 2013, 2016; Dumont et al. 2021).

Population II stars are not an exception and undergo the same type of depletion through the same processes (e.g., Michaud et al. 1984; Richard et al. 2005). Therefore lithium-7 surface abundances observed in Population II stars (known as the Spite plateau, Spite & Spite 1982) are most likely not the initial abundances, hence the discrepancy with a higher cosmological lithium-7 abundance (from BBN). It is interesting to note that many stars are found to have a lower lithium abundance than the lithium plateau (Bonifacio et al. 2007; Cayrel et al. 2008; Sbordone et al. 2010), which can also be explained by stellar models, for example, in the case of carbon-enhanced metal-poor stars with excess in *s*-process elements (CEMP-*s* stars) (e.g., Stancliffe 2009; Deal et al. 2021).

We draw on the self-consistent perturbative analysis formalism introduced in Paper 1 and extended in Paper 2 to revisit the role of stellar depletion in the lithium problem, while simultaneously allowing for time variation of nature's fundamental constants in a broad class of grand unified theory (GUT) scenarios where all the gauge and Yukawa couplings are allowed to vary. We show that the impacts of the two mechanisms can be separately constrained. We start by assuming that a depletion factor relates the cosmological and astrophysical lithium-7 abundances,

$$({}^7\text{Li})_{\text{ast}} = (1 - \Delta)({}^7\text{Li})_{\text{cos}}. \quad (1)$$

Throughout our statistical analyses,  $\Delta$  is allowed to span the entire  $[0, 1]$  range under the assumption of a uniform prior. Clearly, this is a purely phenomenological parameter, and given any pair of cosmological and astrophysical lithium abundances, for which the former is higher than the latter, there will always be a choice of  $\Delta$  that makes the two compatible. In this sense, the observed lithium-7 abundance simply provides a measurement of  $\Delta$ . However, the hypothesis underlying this assumption is that stellar physics mechanisms exist and/or physical transport processes occur in stars that can account for the relevant value of  $\Delta$ . Thus our purpose in introducing Eq. (1) is twofold. First, it allows us to quantify the impact of astrophysical depletion in models, which also allows new physics mechanisms (specifically, through varying fundamental constants here), thereby comparing the possible roles of the two. Second, it provides a convenient way to assess the extent to which stellar physics mechanisms could lead to depletion.

Following the approach of Paper 1 and Paper 2, we performed our statistical likelihood analyses using three different combinations of the four abundances, as described in the following paragraphs.

First, the baseline case uses the abundances of helium-4, deuterium, and lithium-7, which are the three available cosmological abundances. This provides the reference values for the best-fit BBN values for  $\alpha$ .

Second, the extended case adds the helium-3 abundance to the first three abundances. This separation stems from the fact that its observed abundance is local rather than cosmological. As we pointed out in Paper 1 and Paper 2, this has a negligibly small effect on the derived constraints.

Third, the null case, which uses the helium-4, deuterium, and helium-3 abundances, but does not use lithium-7. The motivation for this case is that it provides a useful null test of the BBN sensitivity to the value of the fine-structure constant. In other words, if all the relevant physics is the standard physics, it is expected that the standard value of  $\alpha$  is recovered in this case to some degree of sensitivity that is useful to quantify and compare to other probes. It also provides an indication of the BBN constraints on  $\alpha$  based on the assumption that the lithium problem has an astrophysical solution.

For convenience, we use the terms Baseline, Extended, and Null to denote each of the three combinations when we present the results in figures in the first part of the work. (This facilitates comparisons with the results in Paper 1 and Paper 2.) In the second part and when we summarize results in the text and tables throughout the work, we concentrate on the Baseline case and provide Null case results for comparison when relevant.

The plan of the rest of this work is as follows. We start in Sect. 2 by phenomenologically quantifying the preferred depletion factor  $\Delta$  assuming that the three key cosmological parameters, that is, the neutron lifetime, the number of neutrinos, and the baryon-to-photon ratio, are allowed to vary, but constrained by priors external to BBN. In Sect. 3 we report on the analogous study for GUT scenarios where all the gauge and Yukawa couplings are allowed to vary, confirming the previously reported preference for a higher value of  $\alpha$  in the BBN epoch. In this case, the baryon-to-photon ratio and number of neutrinos are assumed to be fixed at their standard values, while the neutron lifetime is unavoidably affected. Together, these two sections confirm a discrepancy in the values of the baryon-to-photon ratio, or equivalently, the primordial Deuterium abundance, preferred by BBN and cosmic microwave background (CMB) plus baryon acoustic oscillation (BAO) data, which has recently been reported (Pitrou et al. 2021; Yeh et al. 2021). In

**Table 1.** Theoretical and observed primordial abundances.

Abundance	Theoretical	Observed
$Y_p$	$0.24721 \pm 0.00014$	$0.245 \pm 0.003$
$(D/H) \times 10^5$	$2.439 \pm 0.037$	$2.547 \pm 0.025$
$(^3\text{He}/H) \times 10^5$	$1.039 \pm 0.014$	$1.1 \pm 0.2$
$(^7\text{Li}/H) \times 10^{10}$	$5.464 \pm 0.220$	$1.6 \pm 0.3$

**Notes.** The theoretical abundances have been obtained in [Pitrou et al. \(2021\)](#). The observed abundances are the recommended values in the 2020 Particle Data Group BBN review, with representative references being [Aver et al. \(2015\)](#), [Cooke et al. \(2018\)](#), [Banja et al. \(2002\)](#), and [Sbordone et al. \(2010\)](#). We note that strictly speaking, the  $^3\text{He}$  value is not cosmological; see the main text for further discussion.

Sect. 4 we address the lithium problem, showing that the combination of atomic diffusion, rotation, and penetrative convection can bridge the gap between the cosmological abundance and the surface abundances measured in Population II stars. In Sect. 5 we address the Deuterium discrepancy, showing that it (and not the lithium problem) is driving the preference for a higher value of  $\alpha$ , and further quantifying the model dependence of this preference. Finally, we offer some conclusions in Sect. 6.

## 2. Depletion and cosmological parameters

Generically, the sensitivity of the primordial BBN abundances to the various relevant model parameters can be described as

$$\frac{\Delta Y_i}{Y_i} = \sum_j C_{ij} \frac{\Delta X_j}{X_j}, \quad (2)$$

where  $C_{ij} = \partial \ln(Y_i) / \partial \ln(X_j)$  are the sensitivity coefficients. The perturbation is always done with respect to the predicted abundance values in some baseline theoretical model, which in our case is the model that was recently presented in [Pitrou et al. \(2021\)](#). These predicted abundances are listed in Table 1 for convenience, together with the observed abundances as recommended by the BBN review in [Zyla et al. \(2020\)](#). The two are compared using standard statistical likelihood methods, and theoretical and observational uncertainties are added in quadrature. We note that our fiducial model differs from the model used in Paper 1 and Paper 2, which was based on the earlier work of [Pitrou et al. \(2018\)](#). Therefore our results here can be approximately (but not exactly) compared with those of the earlier papers.

In this section we consider the effect of the values of the neutron lifetime  $\tau_n$ , the number of neutrino species  $N_\nu$ , and the baryon-to-photon ratio  $\eta_{10}$  (where for convenience, we defined  $\eta_{10} = \eta \times 10^{10}$ ) on the BBN abundances. The fiducial values of these parameters (which are used as statistical Gaussian priors in the analysis) are

$$\tau_n = 879.4 \pm 0.6 \text{ s} \quad (3)$$

for the neutron lifetime ([Zyla et al. 2020](#)) (see also [Rajan & Desai 2020](#) for a recent discussion of experimental measurements of this lifetime),

$$N_\nu = 2.984 \pm 0.008 \quad (4)$$

for the number of neutrino species, which comes from the LEP measurement ([Zyla et al. 2020](#)), and

$$\eta_{10} = 6.143 \pm 0.038, \quad (5)$$

**Table 2.** Sensitivity coefficients of BBN nuclide abundances on the cosmological parameters in our phenomenological parameterization, defined in the main text.

$C_{ij}$	D	$^3\text{He}$	$^4\text{He}$	$^7\text{Li}$
$t_i$	+0.442	+0.141	+0.732	+0.438
$v_i$	+0.409	+0.136	+0.164	-0.277
$w_i$	-1.65	-0.567	+0.039	+2.08

from the combination of recent CMB (Planck 2018) and BAO data ([Aghanim et al. 2020](#)). For reference, the latter corresponds to the physical baryon density

$$\omega_b = \Omega_b h^2 = \frac{\eta_{10}}{274} = 0.02242 \pm 0.00014. \quad (6)$$

With these assumptions, our perturbative analysis for the BBN abundances has the specific form

$$\frac{\Delta Y_i}{Y_i} = t_i \frac{\Delta \tau_n}{\tau_n} + v_i \frac{\Delta N_\nu}{N_\nu} + w_i \frac{\Delta \eta}{\eta}, \quad (7)$$

where  $t_i$ ,  $v_i$ , and  $w_i$  are the sensitivity coefficients listed in Table 2 that we previously discussed in Paper 2 and references therein. Deuterium is far more sensitive to the baryon fraction than to the neutron lifetime or the number of neutrinos, while the opposite holds for Helium-4. Additionally, we assumed that the cosmological and astrophysical lithium-7 abundances are related through Eq. (1), so that the depletion factor  $\Delta$  becomes a fourth model parameter, together with the relative variations of the three cosmological parameters.

The results of the analysis are depicted in Fig. 1. The best-fit values of our free parameters (with their one standard deviation uncertainties) in the Baseline case are

$$\frac{\Delta \tau_n}{\tau_n} = 0.0000 \pm 0.0007 \quad (8)$$

$$\frac{\Delta N_\nu}{N_\nu} = 0.0004 \pm 0.0022 \quad (9)$$

$$\frac{\Delta \eta_{10}}{\eta_{10}} = -0.0082 \pm 0.0050 \quad (10)$$

$$\Delta = 0.70 \pm 0.07; \quad (11)$$

in the Null case, the first three of these are the same, while  $\Delta$  is obviously not constrained. (On the other hand, if we assume that  $\tau_n$ ,  $N_\nu$ , and  $\eta_{10}$  are fixed at their fiducial values and are not allowed to vary and marginalized, we find  $\Delta = 0.71 \pm 0.07$ .) These lead to the following best-fit theoretical abundances:

$$Y_p = 0.247 \pm 0.001 \quad (12)$$

$$(D/H) \times 10^5 = 2.474 \pm 0.043 \quad (13)$$

$$(^3\text{He}/H) \times 10^5 = 1.044 \pm 0.015 \quad (14)$$

$$(^7\text{Li}/H) \times 10^{10}(\text{Cos}) = 5.370 \pm 0.224 \quad (15)$$

$$(^7\text{Li}/H) \times 10^{10}(\text{Ast}) = 1.611 \pm 0.387. \quad (16)$$

For lithium-7 we separately list the cosmological (primordial) abundance and the corresponding astrophysical abundance, corrected for the preferred 70% depletion. We confirm the result, which was mentioned by [Pitrou et al. \(2021\)](#), that with the latest nuclear physics cross-sections and observed abundances, the

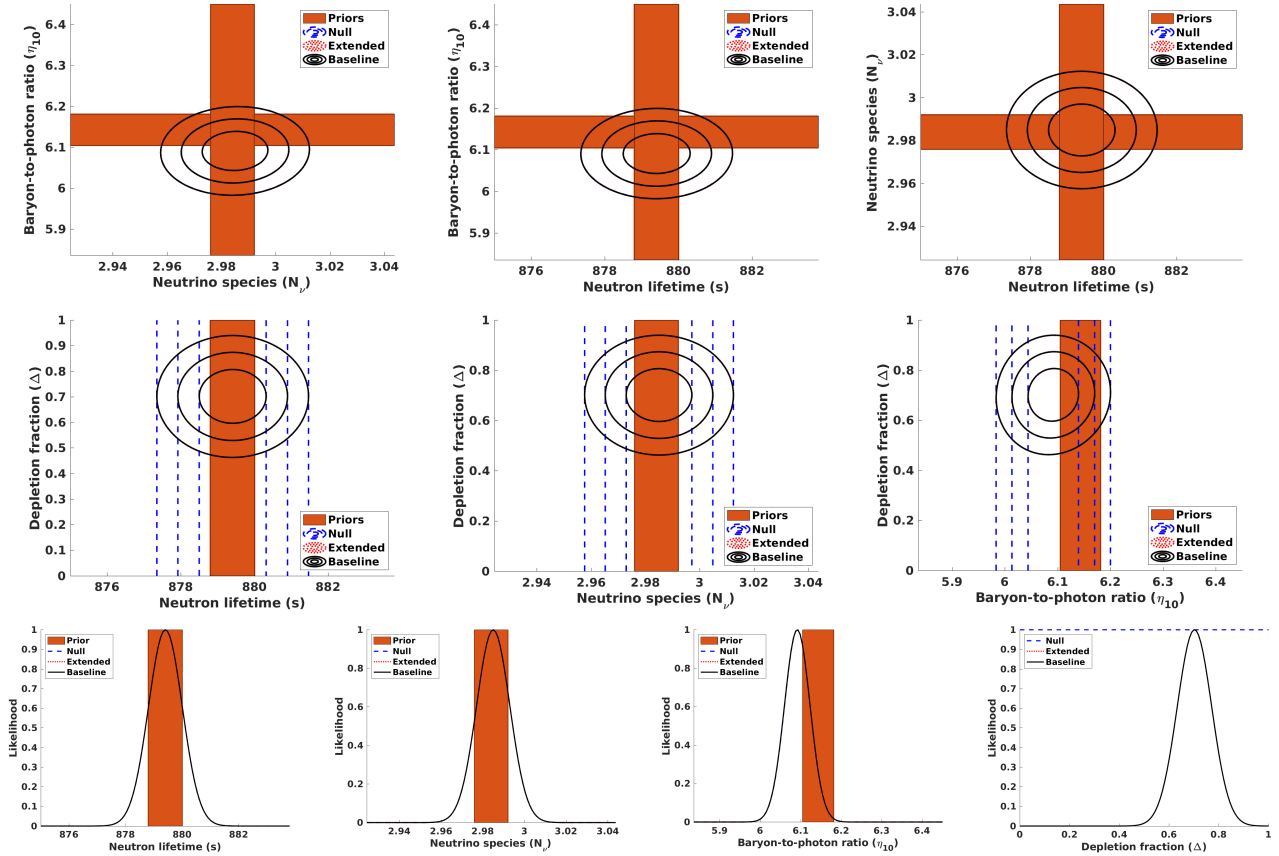


**Fig. 1.** BBN constraints on the lithium-7 phenomenological depletion factor and key cosmological parameters, with remaining parameters marginalized in each case. The  $1\text{-}\sigma$  range corresponding to the priors on cosmological parameters mentioned in the text are also shown for illustration purposes. The two-dimensional planes depict the 68.3, 95.4, and 99.7% confidence levels.

BBN observations prefer a slightly lower  $\eta_{10}$  than was measured by the combination of CMB and BAO observations. Alternatively, this can be phrased as a discrepancy in the Deuterium abundance. On the other hand, different reaction rates were used in Yeh et al. (2021) and in Pisanti et al. (2021), who reported no such discrepancy. In any case, as illustrated in Fig. 1, the discrepancy is only slightly higher than one standard deviation, which means that its statistical significance is limited. We revisit this point below.

### 3. Depletion and varying fundamental constants

The approach introduced Paper 1 and Paper 2 to study BBN with varying fundamental constants is also a perturbative approach. It builds upon earlier work by Muller et al. (2004) and Flambaum & Wirlinga (2007) and subsequent developments by Coc et al. (2007) and Dent et al. (2007) to generically write the relative variations of other couplings as the product of some constant particle physics coefficients and the relative variation of the fine-structure constant. With some reasonable simplifying assumptions, which stem from the work of Campbell & Olive (1995), only two such dimensionless coefficients are needed, one pertaining to electroweak physics (denoted  $S$ ) and the other to strong interactions (denoted  $R$ ). This enables a phenomenological description of a broad range of GUT scenarios. We refer to Paper 1 and Paper 2 for a more detailed description of this formalism. Astrophysical constraints on  $\alpha$  are expressed in terms of a relative variation with respect to the local laboratory value

below,

$$\frac{\Delta\alpha}{\alpha}(z) \equiv \frac{\alpha(z) - \alpha_0}{\alpha_0}, \quad (17)$$

where  $\alpha_0 = 0.0072973525693(11)$  is the local laboratory value.

Under these assumptions, the sensitivity of the primordial BBN abundances to the values of the fundamental constants is therefore expressed as a function of the phenomenological particle physics parameters  $R$  and  $S$  and the relative variation of  $\alpha$ . In other words,

$$\frac{\Delta Y_i}{Y_i} = (x_i + y_i S + z_i R) \frac{\Delta\alpha}{\alpha}; \quad (18)$$

the corresponding sensitivity coefficients are listed in Table 3. The baryon-to-photon ratio and number of neutrinos are assumed to be fixed at their standard values. On the other hand, the neutron lifetime is affected by the  $\alpha$  variation according to

$$\frac{\Delta\tau_n}{\tau_n} = [-0.2 - 2.0 S + 3.8 R] \frac{\Delta\alpha}{\alpha}, \quad (19)$$

but this effect has been included in the computation of these sensitivity coefficients, therefore the neutron lifetime does not appear as an explicit parameter. We refer to Paper 2 for a more detailed discussion.

The phenomenological parameters  $R$  and  $S$  can in principle be taken as free parameters that are to be constrained experimentally or observationally. Our current knowledge of particle physics and unification scenarios suggests that their absolute values can be anything from order unity to several hundreds, with

**Table 3.** Sensitivity coefficients of BBN nuclide abundances on the free unification parameters of our phenomenological parameterization of GUT scenarios, defined in the main text.

$C_{ij}$	D	$^3\text{He}$	$^4\text{He}$	$^7\text{Li}$
$x_i$	+42.0	+1.27	-4.6	-166.6
$y_i$	+39.2	+0.72	-5.0	-151.6
$z_i$	+36.6	-89.5	+14.6	-200.9

**Notes.** The baryon-to-photon ratio and number of neutrinos are assumed to be fixed at their standard values.

**Table 4.** Constraints on  $\Delta\alpha/\alpha$  in the Baseline and Null scenarios for the Unification, Dilaton, and Clocks models, as reported in Paper 1 (Clara & Martins 2020) and Paper 2 (Martins 2021).

Scenarios	Unification	Dilaton	Clocks
Paper 1 (Baseline)	$12.5 \pm 2.9$	$19.9 \pm 4.5$	$2.2^{+15.6}_{-0.6}$
Paper 1 (Null)	$4.6 \pm 3.8$	$5.8 \pm 6.5$	$1.0^{+7.1}_{-0.9}$
Paper 2 (Baseline)	$16.1 \pm 3.9$	$22.6 \pm 5.5$	$2.5^{+3.5}_{-0.5}$
Paper 2 (Null)	$4.6 \pm 5.5$	$3.7 \pm 8.4$	$0.8^{+1.5}_{-0.6}$

**Notes.** The listed values are in ppm and correspond to the best fit in each case and to the range of values within  $\Delta\chi^2 = 4$  of it. The fiducial model used in these papers is not the same as we used here, and the full parameter space was different in the two papers.

$R$  allowed to be positive or negative (although with the former case being the more likely one), while  $S$  is expected to be non-negative.

The analysis of Paper 1 and Paper 2 has identified three models that can provide a solution to the lithium problem (at least in the sense of causing all theoretical and observed abundances to agree to within three standard deviations or less) for the best-fit values of  $\Delta\alpha/\alpha$  listed in Table 4. The fiducial model used in these papers is not the same as we used here, and the full parameter space was different in the two papers.

The first of these is a typical unification scenario, for which we have (Coc et al. 2007; Langacker et al. 2002)

$$R \sim 36, \quad S \sim 160; \quad (20)$$

we refer to this as the Unification model. The second is the dilaton-type model discussed by Nakashima et al. (2010), for which

$$R \sim 109.4, \quad S \sim 0; \quad (21)$$

we refer to this as the Dilaton model. Finally, the Clocks model denotes the general case where the parameters  $R$  and  $S$  are allowed to vary and are then marginalized, in this case, with uniform priors in the range  $R = [0, +500]$ ,  $S = [0, +1000]$ , together with an additional prior coming from local experiments with atomic clocks (Ferreira et al. 2012),

$$(1 + S) - 2.7R = -5 \pm 15. \quad (22)$$

This is therefore a more phenomenological model than the previous two (and has a larger number of free parameters), but serves the purpose of illustrating the range of behaviors that might be found in GUT models, although we should mention that as expected, the results in this case also depend on the choice of priors for  $R$  and  $S$ . This last point has been discussed in Paper 1.

We now repeat the statistical likelihood analysis, allowing for both a variation of fundamental couplings and lithium-7

depletion, for these three models. In this section we assume that the values of the number of neutrino species and the baryon-to-photon ratio are fixed at their standard fiducial values, but the neutron lifetime is implicitly allowed to vary, as pointed out above. The results of this analysis are depicted in Fig. 2 and also summarized in Table 5 for the Baseline case. In the Null case, the depletion fraction is unconstrained, but for comparison, we also list the value of  $\Delta\alpha/\alpha$  in that case.

The observed BBN abundances allow the separate quantification of the role of both effects. The preferred value of the depletion parameter decreases with respect to the parameter obtained with the standard value of  $\alpha$  in Sect. 2 by about one standard deviation. Moreover, there is still a preference for a positive value of  $\Delta\alpha/\alpha$ . Comparison with Table 4 shows that for the Unification and Dilaton models, both the best-fit values and the statistical significance of the preference for the Baseline case are decreased with respect to the values found in Paper 1 and Paper 2, while for the Null case, they are slightly increased. On the other hand, for the Clocks model, the best-fit value for  $\alpha$  agrees with the value found in Paper 1 and Paper 2 in both the Null and the Baseline cases. In this case, the effect of the additional depletion mechanism is manifest in the best-fit values for the phenomenological particle physics parameters  $R$  and  $S$ . Here we find

$$R = 15^{+15}_{-7}, \quad S = 35^{+30}_{-16}, \quad (23)$$

whereas in Paper 2, the best-fit values were

$$R = 40^{+30}_{-10}, \quad S = 100 \pm 30. \quad (24)$$

Although  $R$  and  $S$  are independent parameters in the likelihood analysis, the local prior from atomic clock experiments, see Eq. (22), effectively correlates them. The difference between the two sets of values reflects the fact that in Paper 2 no depletion factor was allowed (effectively,  $\Delta = 0$  was used). Moreover, bearing in mind the slight reduction of the depletion factor when a nonstandard value of  $\alpha$  is allowed, it also shows that although a value of  $\Delta\alpha/\alpha > 0$  alleviates the lithium problem, it does not completely solve it. Instead, a significant depletion factor is still statistically preferred.

The more noteworthy aspect is that unlike the results of Paper 1 and Paper 2, the preferred values for  $\Delta\alpha/\alpha$  are almost identical in the Baseline and Null cases, meaning that the preference for a positive value of  $\Delta\alpha/\alpha$  is not driven by the lithium-7 problem. In other words, even when lithium-7 is not included in the analysis, there is a mild statistical preference for a variation of  $\Delta\alpha/\alpha$  at the few parts-per-million level. Instead, it is driven by the small discrepancy we described in the previous section between the baryon-to-photon ratios inferred from BBN and the corresponding CMB value. In other words, it is driven by the helium-4 and deuterium data. We note that within the standard paradigm, the baryon-to-photon ratio is a constant and has the same value in the BBN and CMB epochs. A different value in the two epochs necessarily implies the presence of new physics.

When lithium-7 is added to the analysis without allowing for the possibility of a depletion mechanism (as was done in Paper 1 and Paper 2), the preferred value of  $\Delta\alpha/\alpha$  increases very significantly with respect to the Null case because a higher value of  $\alpha$  is needed solve the lithium problem per se. On the other hand, if a depletion mechanism is allowed (as in the present work), then this mechanism provides the dominant contribution to address the lithium problem, and the value of  $\Delta\alpha/\alpha$  is very slightly changed with the respect to the Null case. Nevertheless,

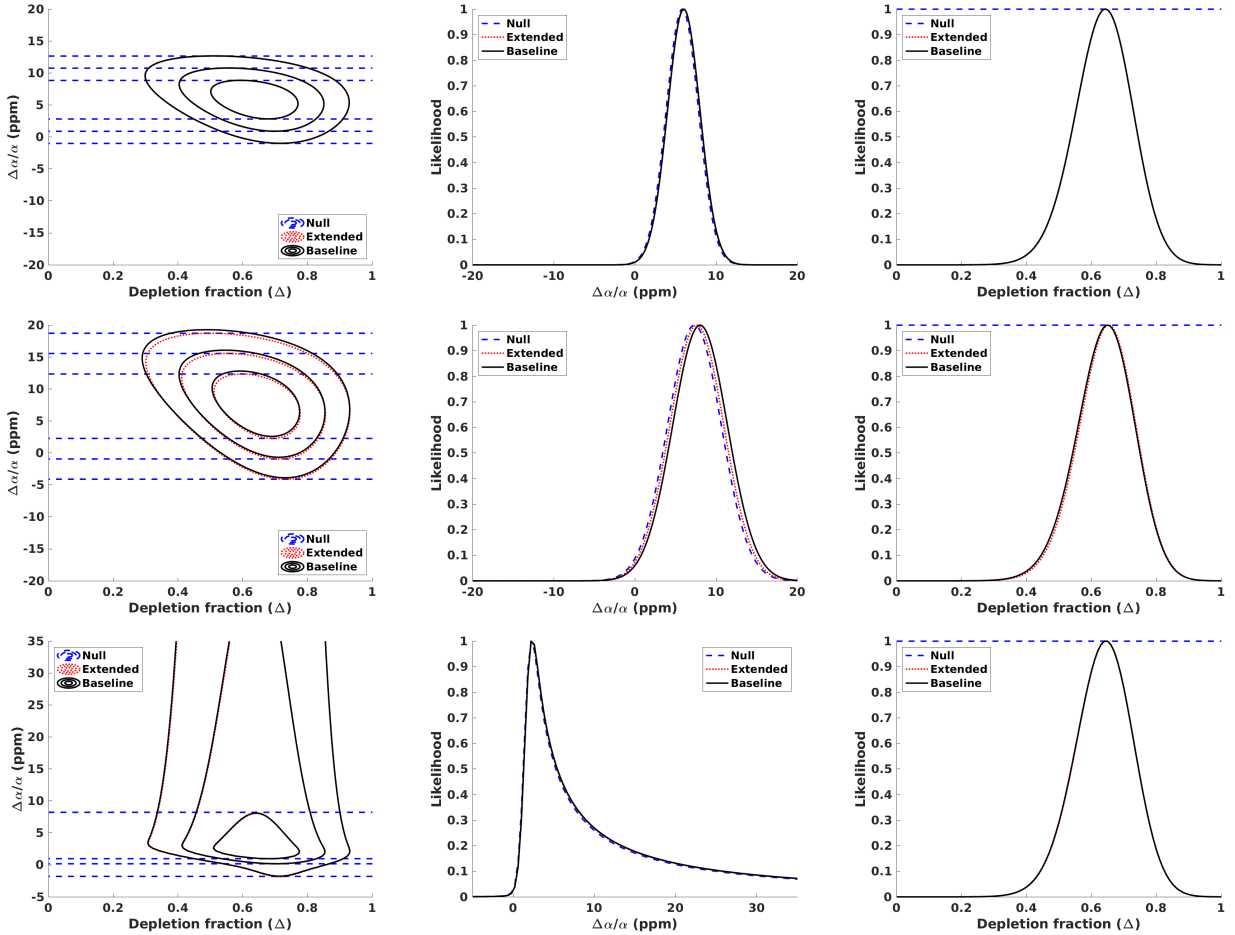


**Fig. 2.** BBN constraints on the fine-structure constant and the lithium-7 phenomenological depletion factor, with remaining parameters marginalized in each case. The two-dimensional planes depict the 68.3, 95.4, and 99.7% confidence levels. Panels in the *first, second, and third* rows correspond to the Unification, Dilaton, and Clocks models.

**Table 5.** Constraints on  $\Delta\alpha/\alpha$  and  $\Delta$  for the Unification, Dilaton, and Clocks models (with the range of values within  $\Delta\chi^2 = 1$  of it, corresponding to the 68.3% confidence level for a Gaussian posterior likelihood), together with the derived nuclide abundances for each of the best-fit models.

Parameter	Unification	Dilaton	Clocks
$\frac{\Delta\alpha}{\alpha}$ (ppm), Null	$5.8 \pm 2.0$	$7.3 \pm 3.3$	$2.2^{+2.4}_{-0.8}$
$\frac{\Delta\alpha}{\alpha}$ (ppm), Baseline	$6.0 \pm 2.0$	$8.0 \pm 3.4$	$2.2^{+2.4}_{-0.8}$
$\Delta$	$0.64 \pm 0.09$	$0.65 \pm 0.09$	$0.64 \pm 0.09$
$Y_p$	$0.247 \pm 0.001$	$0.249 \pm 0.001$	$0.247 \pm 0.002$
$(D/H) \times 10^5$	$2.55 \pm 0.05$	$2.52 \pm 0.05$	$2.45 \pm 0.07$
$(^3\text{He}/H) \times 10^5$	$1.02 \pm 0.02$	$0.96 \pm 0.04$	$1.04 \pm 0.07$
$(^7\text{Li}/H) \times 10^{10}$ (Cos)	$4.42 \pm 0.25$	$4.51 \pm 0.24$	$5.36 \pm 0.26$
$(^7\text{Li}/H) \times 10^{10}$ (Ast)	$1.59 \pm 0.52$	$1.58 \pm 0.52$	$1.92 \pm 0.60$

**Notes.** For lithium-7 we separately list the cosmological (primordial) abundance and the corresponding astrophysical abundance, corrected for the preferred depletion. The results are for the Baseline scenario, with the exception of the first row, which shows the value of  $\Delta\alpha/\alpha$  in the Null case for comparison.

the inclusion of  $\Delta\alpha/\alpha$  is still significant, which is manifest in the fact that the preferred depletion fraction changes with respect to the case discussed in the previous section by about one standard deviation.

One can now obtain a summary plot of the standard theoretical and observed abundances, together with those predicted for the best-fit values of the various models discussed in Sect. 2 and in this section. This can be found in Fig. 3.

It is interesting to note that although the Unification and Dilaton models lead to very similar lithium-7 abundances (a consequence of the fact that this nuclide drives the statistical analysis), they lead to significantly different abundances for the other nuclides, especially for helium-4 and helium-3. Specifically, the Dilaton model leads to a significantly higher helium-4 abundance and a significantly lower helium-3 abundance than the Unification model. The reason is that the Dilaton model,

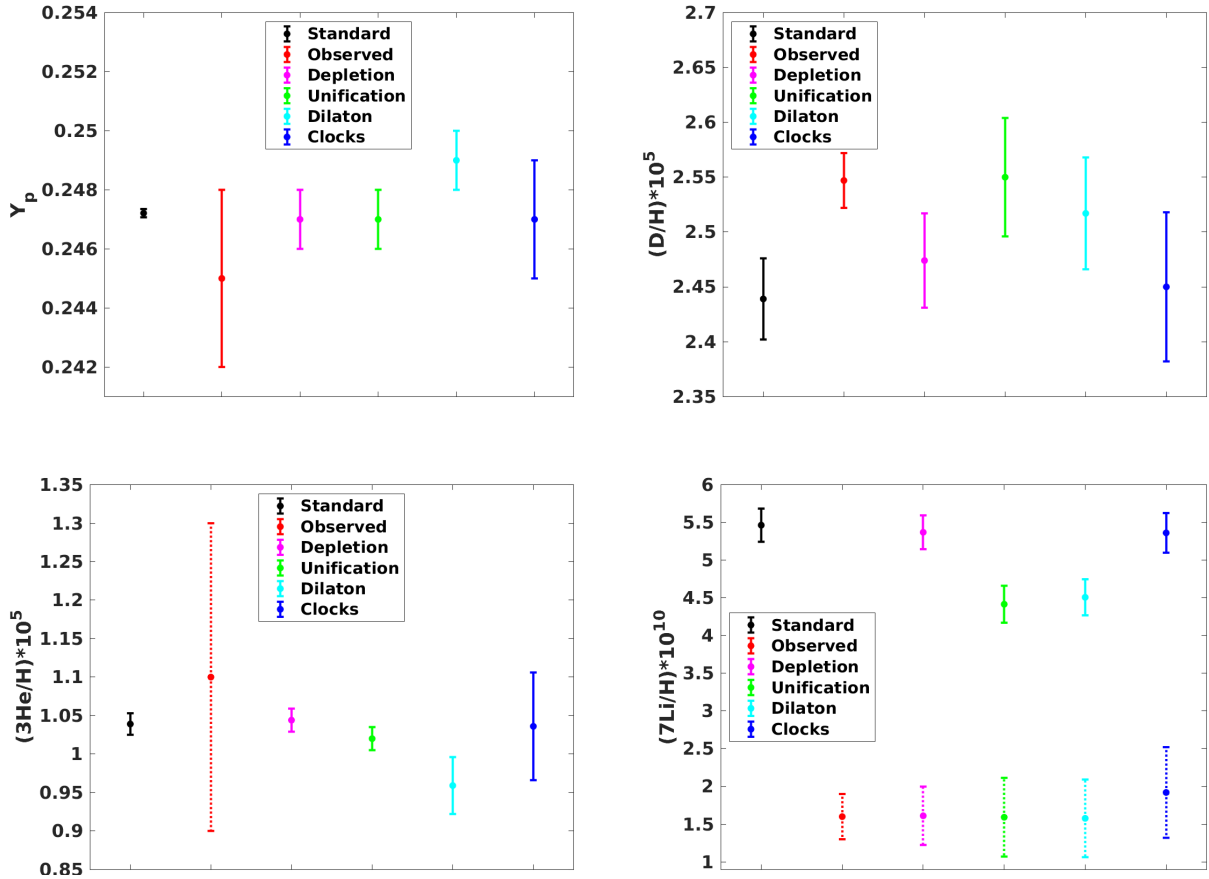


**Fig. 3.** Graphical comparison of the data in Tables 1 and 5 for each of the four nuclides. In each panel the black points are the standard theoretical values of Pitrou et al. (2021), and the red points are the observed abundances. They are listed in Table 1. The magenta points show the best-fit depletion-only model discussed in Sect. 2, and the green, cyan, and blue points are the best fit in the Unification, Dilaton, and Clocks cases discussed in Table 5. The  $1\text{-}\sigma$  uncertainties are depicted in all cases. The lithium-7 panel depicts both the cosmological and astrophysical (depleted) abundances; the latter and the helium-3 observed abundance are shown with dotted error bars to indicate that they are not cosmological.

where  $R$  is comparatively large, contains large positive and negative sensitivity coefficients for helium-4 and helium-3, respectively. The comparison of the three models also confirms the well-known result that for the observationally relevant ratios of the baryon-to-photon ratio, the deuterium and lithium-7 abundances are anticorrelated (Olive et al. 2012; Coc et al. 2015), so that a reduction of the latter abundance leads to an increase of the former. Similarly, an anticorrelation between the helium-4 and helium-3 abundances is recorded, highlighting the fact that an accurate determination of the primordial cosmological abundance would provide a sensitive consistency test of BBN.

#### 4. Stellar depletion and the lithium problem

In this section we assess how realistic the depletion factor  $\Delta$  determined in the previous section is according to stellar evolution theory. We compare  $\Delta$  to predicted lithium-7 depletion in stellar models, including different transport processes of chemical elements.

##### 4.1. Input physics of the stellar models

The depletion of lithium that occurs during the evolution of Population II stars is predicted using the Montreal/Montpellier stellar evolution code (Turcotte et al. 1998a) and Code d’Evolution Stellaire Adaptatif et Modulaire (CESTAM, the “T” stands for Transport: Morel & Lebreton 2008; Marques et al. 2013;

Deal et al. 2018). We used two stellar evolution codes, first to confirm the results, and second because they do not include the same transport processes of chemical elements. The Montréal/Montpellier code has already been used to model Population II stars, and especially lithium surface abundances, including detailed atomic diffusion calculations (e.g., Richard et al. 2005). The CESTAM evolution code also includes atomic diffusion (with independent formalisms, see Deal et al. 2018 for more details) and is able to model the effect of rotation (Marques et al. 2013).

Our Montréal/Montpellier models have the same input physics as the models used by Deal et al. (2021) without accretion. CESTAM models are computed with the same input physics as in Deal et al. (2020), except that the mixing length parameter was set to  $\alpha_{\text{CGM}} = 0.69$  following the Canuto et al. (1996) formalism. The opacity tables are the OP table at fixed chemical composition and not the monochromatic tables (OPCDv3.3, Seaton 2005). We tested that when the additional transport processes were included in the models, the abundance variation was not sufficient to modify the internal structure (especially the size of the surface convective zone). Using simpler opacity tables has then a negligible impact on the lithium surface abundance in the specific framework of this study<sup>1</sup>. No

<sup>1</sup> This approximation of the opacity calculation in presence of transport of chemical elements is not valid in most cases (e.g., Turcotte et al. 1998b; Richard et al. 2001; Théado et al. 2009; Deal et al. 2016, 2018).

**Table 6.** Input physics of the stellar models. All sets include models at 0.55, 0.60, 0.65, 0.70, 0.75, and 0.78  $M_{\odot}$ .

Code	Montréal/Montpellier <sup>(a)</sup>		CESTAM <sup>(b)</sup>					
Model set	1	2	3	4	5	6	7	8
$T_0$ [ $10^6$ K] <sup>(1)</sup>	1.0, 1.32, 1.74, 1.80, 1.90, 2.24	1.60, 1.74, 1.80, 1.90	–	–	–	–	–	–
$v_{\text{ZAMS}}$ [ $\text{km}\cdot\text{s}^{-1}$ ]	–	–	15	15	15	15	15	15
$v_{\text{v,add}}$ [ $\text{cm}^2\cdot\text{s}^{-1}$ ]	–	–	$10^8$	0	$10^8$	$10^8$	$10^8$	$10^8$
$\alpha_{\text{ovi}}$ [ $H_p$ ]	–	–	–	–	0.1	0.3	0.4	0.6
Opacities	OPAL monochromatic <sup>(c)</sup>		OP <sup>(d)</sup>					
Eos	CEFF <sup>(e)</sup>		OPAL2005 <sup>(f)</sup>					
Nuc. react.	Bahcall92 <sup>(g)</sup>		NACRE+LUNA <sup>(h)</sup>					
$\alpha_{\text{conv.}}$	1.66 <sup>(i)</sup>		0.69 <sup>(j)</sup>					
Initial mix.			AGSS09 <sup>(k)</sup>					
$X_{\text{ini}}$			0.7538					
$Y_{\text{ini}}$			0.2461					
$(^7\text{Li}/\text{H})\times 10^{10}$			4.45					
[Fe/H]			–2.31					
$\alpha$ enhanc.			+0.3					
Core ov.			None					

**Notes.** The complete initial chemical composition is available in Deal et al. (2021). <sup>(1)</sup>Reference temperature in the expression of  $D_{\text{turb}}$  (see Eq. (25)). <sup>(i)</sup>Solar calibrated value with the Böhm-Vitense (1958) formalism. <sup>(j)</sup>Solar calibrated value with the Canuto et al. (1996) formalism for models including atomic diffusion.

**References.** <sup>(a)</sup>Turcotte et al. (1998a). <sup>(b)</sup>Morel & Lebreton (2008), Marques et al. (2013), Deal et al. (2018). <sup>(c)</sup>Iglesias & Rogers (1996), tables not public. <sup>(d)</sup>Seaton (2005). <sup>(e)</sup>Christensen-Dalsgaard & Daeppen (1992). <sup>(f)</sup>Rogers & Nayfonov (2002). <sup>(g)</sup>Bahcall & Pinsonneault (1992). <sup>(h)</sup>Angulo (1999) + Imbriani et al. (2004) for  $^{14}\text{N}(p, \gamma)^{15}\text{O}$ . <sup>(k)</sup>Asplund et al. (2009).

core overshoot is taken into account, and the initial chemical composition is that of Montréal/Montpellier models ( $[\text{Fe}/\text{H}]_{\text{ini}} = -2.31$  dex). Considering a wider range of initial chemical composition would not affect the conclusion of this work because at these low metallicities, the structure variations are small (especially the size of the surface convective zone, which is important for lithium surface abundances variations; see, e.g., Richard et al. 2002). It should be noticed that with these models, no additional depletion or dispersion for the lower metallicities is predicted, contrarily to what has been observed (Sbordone et al. 2010). The mechanism that might explain this behavior is still unknown. The models were computed with masses between 0.55 and 0.78  $M_{\odot}$ . All models were on the main sequence at 12.5 Gyr and covered a range of effective temperature [5000,6500] K, typical of observed main-sequence Population II stars. The physics of all models is presented in Table 6.

#### 4.2. Transport processes of chemical elements

We computed stellar models including different transport processes of chemical elements. In particular, they all affect the transport of lithium-7 and therefore play a role in the lithium depletion. Most of the processes considered in this study have been extensively described by Dumont et al. (2021) and references therein. In the following, we briefly describe the impact of the processes on lithium depletion and the prescriptions we use in the stellar models. As the aim of this section is to show that the  $\Delta$  depletion factor can be explained by stellar physics, we only included simple modeling approaches for some of the processes addressed below. Including more realistic modeling is the next natural step of this study.

**Convection.** All models include convection using the Schwarzschild criterion. In convective zones, the transport of chemical elements is very efficient and fully homogenizes the

chemical composition. If the bottom part of the convective zone has a temperature close to or higher than the temperature at which lithium is destroyed by proton capture ( $\sim 2.5 \times 10^6$  K), lithium is efficiently depleted. Convective boundaries are defined by the Schwarzschild criterion (Schwarzschild 1958) (or Ledoux criterion, Ledoux 1947) in stellar models. It has been shown that convective plumes can penetrate the radiative zone and then extend the mixing of chemical elements beyond the standard convection criteria (e.g., Zahn 1991; Baraffe et al. 2017). If this extension of the mixing reaches the region in which lithium is destroyed by proton capture, this will also lead to lithium depletion. For the models in this study, we include a simple constant step extension of the surface convective zone  $\alpha_{\text{ovi}}$  in pressure scale-height units ( $H_p$ ). More sophisticated approaches exist (see Dumont et al. 2021, for an overview).

**Atomic diffusion.** All models also include atomic diffusion, which is a selective microscopic transport process. It occurs in every star and is the consequence of the internal gradients of pressure, temperature, and concentration (Michaud et al. 2015). It is efficient in radiative zones. This is mainly the competition between gravity, which causes elements to move toward the center of stars, and radiative acceleration, which causes elements move toward the surface of stars. For the stellar models used in this study, radiative acceleration on lithium is negligible. The transport of lithium by atomic diffusion is dominated by the gravitational settling.

**Parameterized turbulent diffusion coefficient.** Atomic diffusion alone cannot explain the lithium surface abundance of star. Competing transport processes need to be included. It is possible to account for them using a parameterized turbulent diffusion coefficient. Such a coefficient was already used and calibrated to reproduce the lithium surface abundance in Population II stars (Richard et al. 2005; Deal et al. 2021) and in clusters (e.g., Gruyters et al. 2013, 2016; Korn et al. 2007). The turbulent

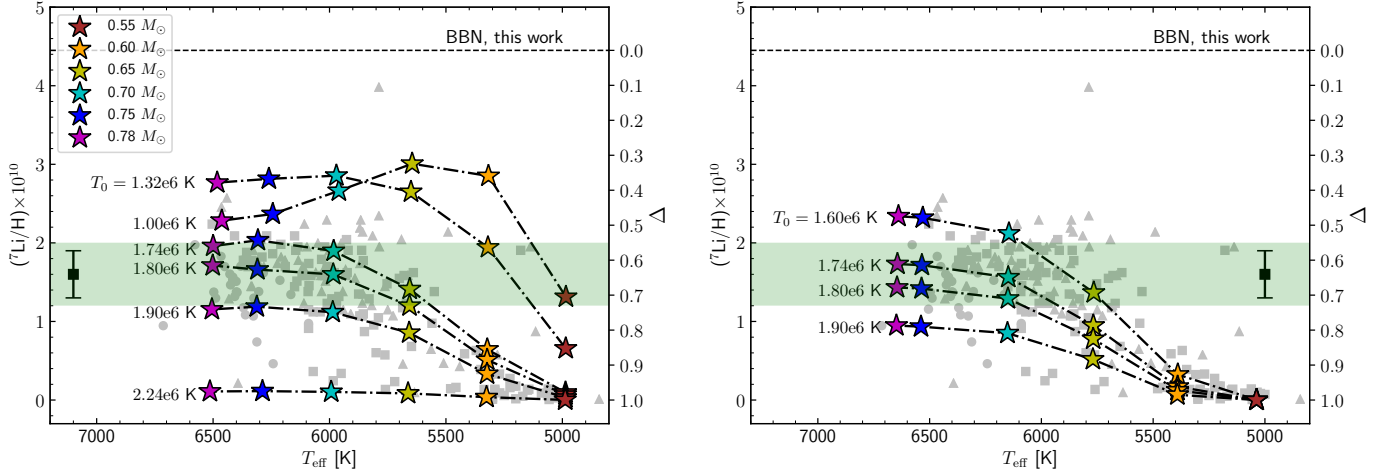


**Fig. 4.** Lithium abundance according to the effective temperature for Montréal/Montpellier models (model set 1, *left panel*) and CESTAM models (model set 2, *right panel*) at 12.5 Gyr, taking into account different  $T_0$  values for the parameterized turbulent diffusion coefficient. The corresponding  $\Delta$  values are shown on the right y-axis. The gray symbols are observed lithium abundances from [Sbordone et al. \(2010\)](#) (circles), [Bonifacio & Molaro \(1997\)](#) (triangles), and the SAGA database (<http://sagadatabase.jp/>, [Suda et al. 2008, 2011](#); [Yamada et al. 2013](#); [Suda et al. 2017](#)) (squares). The black square with error bars represents the standard value for the lithium plateau ([Sbordone et al. 2010](#)). The green area represents the range of  $\Delta$  values found in Sect. 3.

diffusion coefficient is expressed as

$$D_{\text{turb}} = 400 \times D_{\text{He}}(T_0) \left( \frac{\rho(T_0)}{\rho} \right)^3, \quad (25)$$

where  $T_0$  is a reference temperature.  $D_{\text{He}}(T_0)$  is the diffusion coefficient of helium at the reference point<sup>2</sup>,  $\rho$  is the local density, and  $\rho(T_0)$  is the density at the reference point. The only free parameter of this parameterization is  $T_0$ . The way this parameterization is made, the transport of chemical elements is very efficient for internal temperatures smaller than  $T_0$  (i.e., the chemical composition is homogenized from the surface down to  $T_0$ ). For temperatures higher than  $T_0$ , the mixing decreases rapidly as a function of  $\rho^{-3}$ . The higher  $T_0$ , the deeper the efficient mixing region.

**Rotation-induced mixing.** The transport of chemical elements induced by rotation is one of the processes that competes with atomic diffusion. It has an important impact on chemical elements and especially on lithium (e.g., [Charbonnel & Talon 1999](#); [Talon 2008](#); [Dumont et al. 2021](#)). Rotation-induced mixing is mainly driven by the shear instability and the meridional circulation. The differences between the models of this study and those of [Deal et al. \(2020\)](#) are the horizontal diffusion coefficient ( $D_h$ , from [Mathis et al. 2018](#)) and an additional vertical viscosity  $\nu_v = 10^8 \text{ cm}^2 \text{ s}^{-1}$  as calibrated by [Ouazzani et al. \(2019\)](#) to take into account the fact that the current rotation theory underestimates the transport of angular momentum. We also tested lower values of  $\nu_v$ . All models including rotation have a rotation speed at the ZAMS  $v_{\text{ZAMS}} = 15 \text{ km}^{-1}$ . See [Marques et al. \(2013\)](#) for a detailed description of the modeling of rotation in CESTAM.

#### 4.3. Parameterized turbulent transport and atomic diffusion

We first estimated the required transport of chemical elements to explain the  $\Delta$  depletion factor using the parametric turbulent

<sup>2</sup> The diffusion coefficient of helium can be easily calculated using this approximate formula:  $D_{\text{He}} = 3.3 \times 10^{-15} T_0^{2.5} / [4\rho \ln(1 + 1.125 \times 10^{-16} T_0^3 / \rho)]$ .

diffusion described in Sect. 4.2 and atomic diffusion. This kind of approach has been used to study lithium surface abundances of Population II stars (e.g., [Richard et al. 2005](#); [Deal et al. 2021](#)).

The left panel of Fig. 4 shows the lithium surface abundance at 12.5 Gyr in stellar models computed with the Montréal/Montpellier stellar evolution code, including atomic diffusion and different parameterizations of the turbulent diffusion coefficient (model set 1). The models are computed with an initial primordial lithium abundance  $(^7\text{Li}/\text{H}) \times 10^{10} = 4.45$ , following the values of Table 5 for the Unification and Dilaton models. Lithium depletion is higher for the lower masses because of a deeper surface convective zone, that is, close to the region in which lithium is destroyed by nuclear reactions. The higher  $T_0$ , the deeper the turbulent mixing, leading to stronger depletion. The lower  $T_0$ , the stronger the effect of atomic diffusion, that is, the turbulent mixing is not strong enough to balance it. Therefore for  $T_0 = 1.0 \times 10^6 \text{ K}$ , the depletion is higher at  $0.78$  than  $0.65 M_\odot$ . Observations and the range of  $\Delta$  values previously determined are well reproduced by the models for the whole effective temperature range for  $T_0$  values between  $1.74 \times 10^6$  and  $1.90 \times 10^6 \text{ K}$ .

The CESTAM models (right panel of Fig. 4, model set 2) show similar surface abundances, with a slight shift in the  $T_0$  values and in effective temperatures. This difference comes from the different input physics (including the equation of state, opacity tables, and nuclear reaction rates) between the two stellar evolution codes. At a given  $T_0$  value, the difference in lithium abundance is about 10% at most, which does not affect the conclusion of this study. This justifies our confidence in using CESTAM models. In the following subsections, we assess the possible physical processes that cause this turbulent transport.

#### 4.4. Rotation-induced mixing and atomic diffusion

In this section we assess whether the  $\Delta$  depletion factor is linked to the combination of rotation-induced mixing and atomic diffusion. Figure 5 shows two sets of models (sets 3 and 4) in which the two processes are included. In one case, rotation is almost solid (set 3, with  $\nu_{v,\text{add}} = 10^8 \text{ cm}^2 \text{ s}^{-1}$ ), and in the other case, the internal rotation is differential using the standard theory for

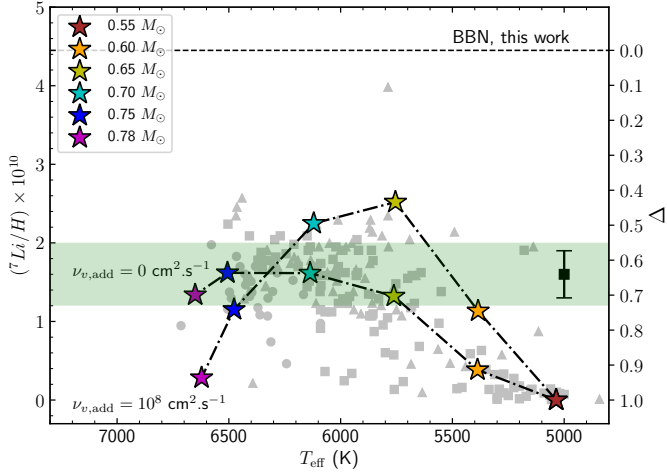


**Fig. 5.** Lithium abundance according to the effective temperature for stellar models of sets 3 and 4 at 12.5 Gyr, taking into account different  $\nu_{v,\text{add}}$  values. Same legend as in Fig. 4 for the other symbols and the green area.

rotation (set 4, with  $\nu_{v,\text{add}} = 0 \text{ cm}^2 \text{ s}^{-1}$ ). The models with an internal differential rotation agree very well with the observations. We tested higher initial rotation speeds for the models with quasi-solid rotation, and the results are very similar. The rotation speed does not play a major role for the transport of chemicals in this specific case.

Helio- and asteroseismology (study of the oscillation of the Sun and stars) also allows us to probe the internal rotation of stars. It has been shown that the internal rotation of the Sun is nearly uniform in the radiative zone at least down to  $R = 0.2 R_{\odot}$  (e.g., Kosovichev 1988; García et al. 2007). Solar models accounting for standard rotation predict a high degree of radial differential rotation (e.g., Eggenberger et al. 2005). The same conclusions are reached when other stars are compared for which we can access the core rotation (e.g., Tayar & Pinsonneault 2013; Deheuvels et al. 2014; Ouazzani et al. 2019). This indicates that of sets 3 and 4, the more realistic models are those of set 3. This implies that the lithium surface abundances of Population II cannot be explained by the combined effect of atomic diffusion and rotation. The same kind of conclusion has previously been obtained for other types of stars (e.g., Deal et al. 2020).

#### 4.5. Penetrative convection, rotation-induced mixing, and atomic diffusion

In this section we assess whether the  $\Delta$  depletion factor can be accounted for by the combination of penetrative convection, rotation-induced mixing, and atomic diffusion. Figure 6 shows four sets of models (set 5, 6, 7, and 8) in which the three processes are included. The four sets cover the range of observed lithium surface abundances well up to an effective temperature of about 6000 K. The values of penetrative convection considered in the models are consistent with what has been determined for the Sun ( $\alpha_{\text{ovi}} \sim 0.37 H_p$ , Christensen-Dalsgaard et al. 2011). For the hotter (more massive) stars, an additional transport process is probably needed to reduce the lithium depletion induced by atomic diffusion. It is possible that the amount of penetrative convection is higher for the more massive stars, which could also cause the models to agree better with the observation. A more realistic treatment of this process could also improve the agreement. Penetrative convection was also invoked in another

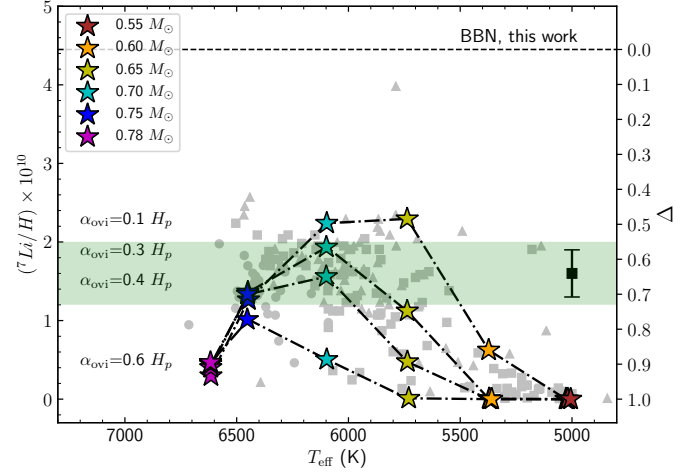


**Fig. 6.** Lithium abundance according to the effective temperature for stellar models of sets 5, 6, 7, and 8, all at 12.5 Gyr, taking into account different  $\alpha_{\text{ovi}}$  values. Same legend as in Fig. 4 for the other symbols and the green area.

scenario to explain lithium abundances in Population II stars (e.g., Fu et al. 2015).

#### 4.6. A minimum astrophysical depletion?

It is interesting to note that a minimum depletion is obtained in the models presented in Sect. 4.5, which is about  $\Delta_{\text{min}} = [0.4; 0.5]$ . From the point of view of stellar modeling, the transport process with the more accurate modeling that leads to the lowest lithium depletion (for masses of about  $0.60\text{--}0.70 M_{\odot}$ ) is atomic diffusion. The efficiency of atomic diffusion strongly depends on the internal structure of stars, and especially on the size of the surface convective zone. The prediction of the minimum depletion of lithium that is expected from stellar models that only include atomic diffusion is then subject to the input physics of the models (including opacity tables, equations of state, convection theory, nuclear reaction rates, etc.). This is less the case when other competing transport processes are taken into account (see the comparison in Fig. 4). In this context, it is difficult to provide a strong constraint on the minimum lithium depletion expected from stellar models. As an example, for the input physics considered in this paper, we find  $\Delta_{\text{min}} = [0.25; 0.40]$  for models that only include atomic diffusion. The only robust conclusion we can draw at this point is that  $\Delta_{\text{min}} > 0$  in all models that include expected transport processes (i.e., at least atomic diffusion).

Overall, we have shown that lithium surface abundances of Population II stars, as well as the range of  $\Delta$  values determined in Sect. 3, are well reproduced by models that include atomic diffusion, a nearly uniform rotation, and some amount of penetrative convection, even if our modeling of the latter and of the missing transport of angular momentum has been somewhat simple. A more realistic modeling of these processes and a systematic study of the effect of the different input physics (opacity tables, equation of states, convection theory, nuclear reaction rates, etc.) are needed to draw stronger conclusions, but our work suffices to show that transport processes of chemical elements in stars not only need to be considered when the lithium problem is addressed, but are also very probable candidates to solving it.

**Table 7.** Sensitivity coefficients of BBN nuclide abundances on the free parameters of our full phenomenological parameterization, defined in Eq. (26) in the main text.

$C_{ij}$	D	$^3\text{He}$	$^4\text{He}$	$^7\text{Li}$
$x_{n,i}$	+42.1	+1.30	-4.5	-166.5
$y_{n,i}$	+40.1	+2.00	-3.5	-150.7
$z_{n,i}$	+34.9	-90.0	+11.8	-202.6
$t_i$	+0.442	+0.141	+0.732	+0.438
$v_i$	+0.409	+0.136	+0.164	-0.277
$w_i$	-1.65	-0.567	+0.039	+2.08

## 5. Varying fundamental constants and the Deuterium discrepancy

After identifying the small discrepancy between the baryon-to-photon ratios inferred from BBN and the CMB value as the origin of the preference for a nonstandard value of  $\alpha$ , we assess the relative contributions of the helium-4 and deuterium data to this result.

To this end, we repeated the analysis both for the case in which only the deuterium abundance is used and for the case in which both deuterium and helium-4 are used. For each of these, we further considered two sub-cases, either keeping the cosmological parameters (i.e., the neutron lifetime, the number of neutrinos, and the baryon-to-photon ratio) fixed at their best-fit values introduced in Sect. 2, or letting these parameters vary (with the previously described priors) and then marginalizing them.

In the first case, the parameter space is summarized by Eq. (18) and the relevant sensitivity coefficients are given in Table 3. In the second case, the parameter space is wider:

$$\frac{\Delta Y_i}{Y_i} = (x_{n,i} + y_{n,i}S + z_{n,i}R) \frac{\Delta\alpha}{\alpha} + t_i \frac{\Delta\tau_n}{\tau_n} + v_i \frac{\Delta N_\nu}{N_\nu} + w_i \frac{\Delta\eta}{\eta}. \quad (26)$$

As previously mentioned, a variation of  $\alpha$  itself impacts the neutron lifetime. Unlike in Sect. 3, here we explicitly separate this effect from the rest of the effects of the  $\alpha$  variation. This means that the  $\alpha$ -related sensitivity coefficients will change, and we have highlighted this point by adding the  $n$  subscript in the previously defined sensitivity coefficients  $x$ ,  $y$ , and  $z$ . For completeness, all these sensitivity coefficients are reproduced in Table 7.

The results of our analysis with the deuterium and helium-4 abundances are summarized in Fig. 7 and Table 8. The helium-4 abundances can be usefully compared with the Baseline and Null cases reported in Table 5.

First and foremost, we confirm that the preference for  $\Delta\alpha/\alpha > 0$  is driven by the Deuterium results, and the top panels of Fig. 7 also clearly show that this is due to the positive correlation between  $\Delta\alpha/\alpha$  and the baryon-to-photon ratio  $\eta$ , although the strength of this correlation depends on the model. Second, we find that the Helium-4 abundance plays a relatively minor role, but one that again depends on the assumed model.

Specifically, for the Unification and Clocks model, the results in Table 8 are fully consistent with those for the previously discussed Baseline and Null cases. The positive correlation of  $\Delta\alpha/\alpha$  and  $\eta$  is relatively mild. In these circumstances, helium-4 does not affect the constraints on  $\Delta\alpha/\alpha$  noticeably, while allowing the cosmological parameters to vary and marginalizing them simply increases the statistical uncertainties and therefore decreases the significance of the  $\Delta\alpha/\alpha > 0$  preference.

On the other hand, for the Dilaton model, the results are more sensitive to the assumptions underlying the analysis. On the one hand, the stronger positive correlation between  $\Delta\alpha/\alpha$  and  $\eta$  means that regardless of whether  $\eta$  is allowed to vary, it has a mild but discernible impact even when only deuterium is used in the analysis. On the other hand, the inclusion of helium-4 significantly lowers the preferred value of  $\Delta\alpha/\alpha$  because this model tends to overpredict the helium-4 abundance, as shown in Fig. 3. Again, this shows the potential of BBN as a precision test of these theoretical scenarios.

## 6. Conclusions

We have provided an updated analysis of BBN constraints in the framework of a wide class of grand unified theory scenarios (Clara & Martins 2020; Martins 2021), in particular addressing the long-standing lithium problem (Fields 2011; Mathews et al. 2020) and the more recently noted Deuterium discrepancy (Pitrou et al. 2021). For the first, we highlighted and quantified the astrophysical mechanisms that can provide a solution, while for the second, we identified a possible indication of new physics, specifically a mild (two to three standard deviations) preference for  $\Delta\alpha/\alpha > 0$ , at the parts-per-million level. These variations would be consistent with all other current  $\alpha$  constraints (Martins 2017).

We note that the Deuterium discrepancy identified by Pitrou et al. (2021) has not been confirmed by other authors (Yeh et al. 2021; Pisanti et al. 2021) who relied on different reaction rates. From a statistical point of view, the main difference is that the uncertainties in the theoretical abundances obtained by Pitrou et al. (2021) are smaller than those of other analyses, although there are also small differences in the preferred values of these abundances. While we did not repeat our analysis with these different reaction rates (and the corresponding theoretical abundances inferred from them), we would expect that the propagation of the larger uncertainties on the theoretical side would lead to larger uncertainties on the fine-structure constant measurements, reducing the statistical significance of the preference for a nonstandard value.

We have quantitatively determined the amount of a lithium depletion that would be needed to solve the lithium problem and searched for depletion mechanisms that occur during the evolution of stars, namely, the transport processes of chemical elements. We showed that taking atomic diffusion, rotation-induced mixing, and some amount of penetrative convection into account in stellar models (consistent with the amount determined from solar observation, Christensen-Dalsgaard et al. 2011), we can reproduce the lithium surface abundances of Population II stars. More realistic modeling of some of the processes (especially the penetrative convection and the missing transport of angular momentum) are required to draw a more robust conclusion. We showed the necessity of including the stellar contribution to the lithium problem, however. Transport processes of chemical elements most likely dominate the contribution to the solution of this problem.

The stellar models were computed with the best-fit value for the initial primordial lithium abundance derived in this study, in the context of the GUT scenarios under consideration, of approximately  $(^7\text{Li}/\text{H}) \times 10^{10} = 4.45$ . Considering stellar models with higher initial primordial lithium, as obtained in the standard BBN model (i.e.,  $(^7\text{Li}/\text{H}) \times 10^{10} = 5.46$ ) would not strongly impact our conclusions. This difference would only lead to the need of a slightly larger amount of penetrative convection to explain the additional depletion. This also shows that from the

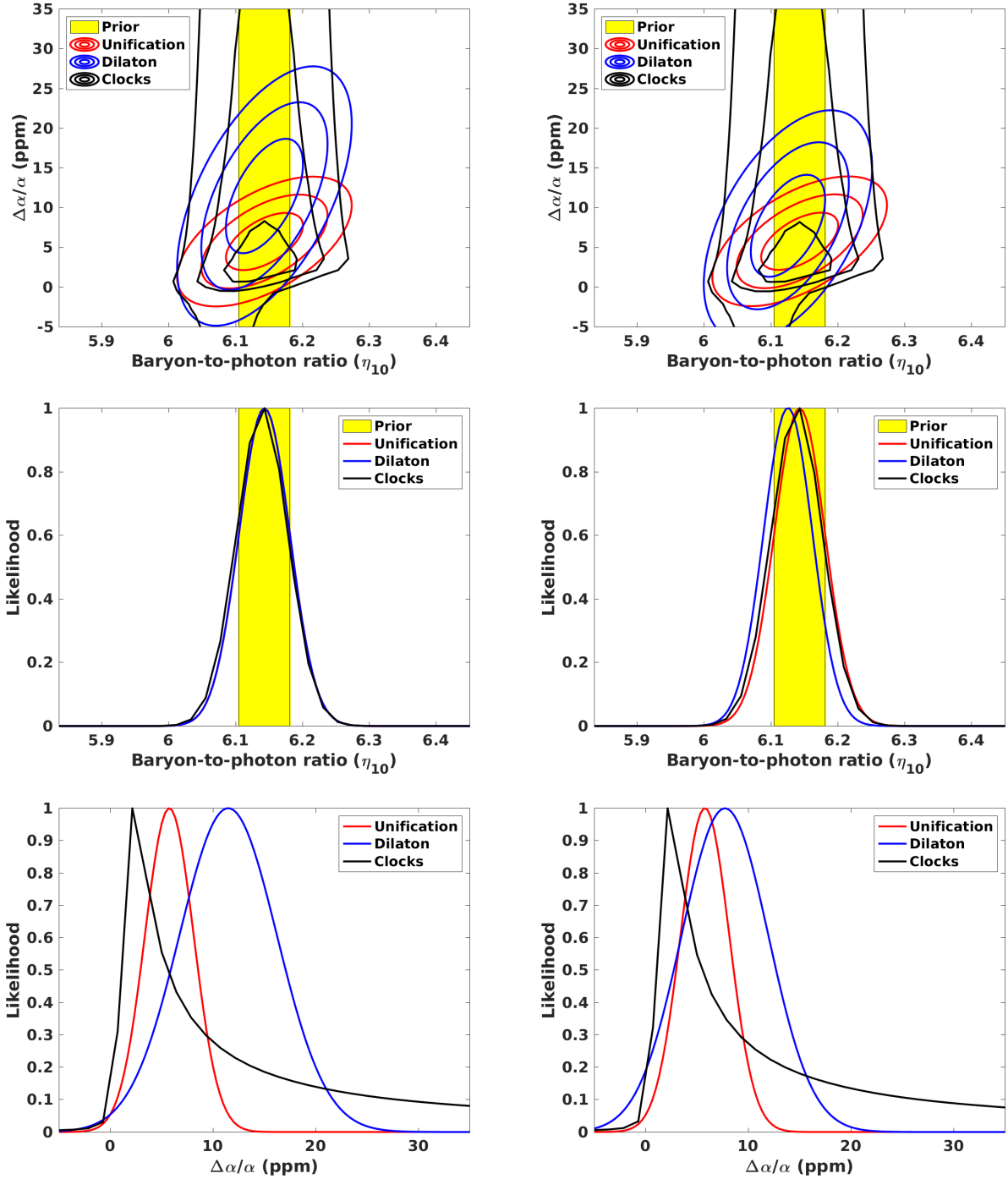


**Fig. 7.** BBN constraints on the fine-structure constant and the baryon-to-photon ratio, with remaining parameters marginalized in each case. The two-dimensional planes depict the 68.3, 95.4 and 99.7 percent confidence levels. *Left side panels:* results for Deuterium only, and *right side panels:* results for Deuterium plus Helium-4.

point of view of stellar physics, the accuracy of the primordial lithium abundance is crucial to constrain the transport of chemical elements in metal-poor stars.

Currently, only two primordial (cosmological) abundances are well known, those of Deuterium and Helium-4. It is therefore highly desirable to close the loop through a cosmological measurement of the Helium-3 abundance, especially given the anticorrelation of the helium-4 and helium-3 abundances. This would enable a key consistency test of the underlying physics, which will be particularly crucial should evidence for new physics be confirmed.

Our analysis highlights the role of BBN as a consistency test of the standard cosmological paradigm and as a sensitive probe of new physics. For the broad phenomenological but physically motivated class of models we considered, improving the observed abundances of Deuterium and Helium-4 by a factor of 2–3 will provide a stringent test, and in particular will definitively confirm or rule out the present tentative evidence for the  $\alpha$  variation. This is a highly compelling science case for the forthcoming Extremely Large Telescope (Liske et al. 2014; Marconi et al. 2020) if it has an efficient blue wavelength coverage.

**Table 8.** Constraints on  $\Delta\alpha/\alpha$  for the Unification, Dilaton, and Clocks models (with the range of values within  $\Delta\chi^2 = 1$  of it, corresponding to the 68.3% confidence level for a Gaussian posterior likelihood), obtained from the Deuterium-only and Deuterium plus Helium4 abundances, and with the values of the other relevant parameters (neutron lifetime, number of neutrinos, and baryon-to-photon ratio) fixed or marginalized as described in the main text.

Data	Parameters	Unification	Dilaton	Clocks
D only	Fixed	$5.8 \pm 2.0$	$10.9 \pm 3.8$	$2.3^{+2.1}_{-0.8}$
D only	Marginalized	$5.7 \pm 2.7$	$11.3 \pm 4.8$	$2.1^{+2.9}_{-0.9}$
D + He4	Fixed	$5.8 \pm 2.0$	$7.7 \pm 3.4$	$2.2^{+2.4}_{-0.8}$
D + He4	Marginalized	$5.7 \pm 2.7$	$7.7 \pm 4.3$	$2.1^{+2.7}_{-0.9}$

*Acknowledgements.* This work was supported by FCT—Fundação para a Ciência e a Tecnologia through national funds (grants PTDC/FIS-AST/28987/2017 and PTDC/FIS-AST/30389/2017) and by FEDER—Fundo Europeu de Desenvolvimento Regional funds through the COMPETE 2020—Operacional Programme for Competitiveness and Internationalisation (POCI-01-0145-FEDER-028987 and POCI-01-0145-FEDER-030389). Additional funds were provided by FCT/MCTES through the research grants UIDB/04434/2020 and UIDP/04434/2020. MD is supported by national funds through FCT in the form of a work contract. CJM gratefully acknowledges useful discussions with Brian Fields and Cyril Pitrou in the context of the ESO Cosmic Duologue on BBN, and with Paolo Molaro. We thank an anonymous referee for valuable comments which helped to improve the paper.

## References

- Aghanim, N., Akrami, Y., Ashdown, M., et al. 2020, *A&A*, **641**, A6
- Aguado, D. S., Hernández, J. I. G., Allende Prieto, C., & Rebolo, R. 2019, *ApJ*, **874**, L21
- Angulo, C. 1999, *Am. Inst. Phys. Conf. Ser.*, **495**, 365
- Asplund, M., Grevesse, N., Sauval, A. J., & Scott, P. 2009, *ARA&A*, **47**, 481
- Aver, E., Olive, K. A., & Skillman, E. D. 2015, *JCAP*, **1507**, 011
- Bahcall, J. N., & Pinsonneault, M. H. 1992, *Rev. Mod. Phys.*, **64**, 885
- Bania, T. M., Rood, R. T., & Balser, D. S. 2002, *Nature*, **415**, 54
- Baraffe, I., Pratt, J., Goffrey, T., et al. 2017, *ApJ*, **845**, L6
- Böhm-Vitense, E. 1958, *ZAp*, **46**, 108
- Bonifacio, P., & Molaro, P. 1997, *MNRAS*, **285**, 847
- Bonifacio, P., Molaro, P., Sivarani, T., et al. 2007, *A&A*, **462**, 851
- Brown, J. M., Garaud, P., & Stellmach, S. 2013, *ApJ*, **768**, 34
- Campbell, B. A., & Olive, K. A. 1995, *Phys. Lett. B*, **345**, 429
- Canuto, V. M., Goldman, I., & Mazzitelli, I. 1996, *ApJ*, **473**, 550
- Cayrel, R., Steffen, M., Bonifacio, P., Ludwig, H. G., & Caffau, E. 2008, *Nuclei in the Cosmos (NIC X)*, 12
- Charbonnel, C., & Talon, S. 1999, *A&A*, **351**, 635
- Charbonnel, C., Vauclair, S., Maeder, A., Meynet, G., & Schaller, G. 1994, *A&A*, **283**, 155
- Christensen-Dalsgaard, J., & Daeppen, W. 1992, *A&ARv.*, **4**, 267
- Christensen-Dalsgaard, J., Monteiro, M. J. P. F. G., Rempel, M., & Thompson, M. J. 2011, *MNRAS*, **414**, 1158
- Clara, M., & Martins, C. 2020, *A&A*, **633**, L11
- Coc, A., Nunes, N. J., Olive, K. A., Uzan, J.-P., & Vangioni, E. 2007, *Phys. Rev. D*, **76**, 023511
- Coc, A., Petitjean, P., Uzan, J.-P., et al. 2015, *Phys. Rev. D*, **92**, 123526
- Cooke, R. J., Pettini, M., & Steidel, C. C. 2018, *ApJ*, **855**, 102
- Damour, T., Piazza, F., & Veneziano, G. 2002, *Phys. Rev. Lett.*, **89**, 081601
- Deal, M., Richard, O., & Vauclair, S. 2016, *A&A*, **589**, A140
- Deal, M., Alecian, G., Lebreton, Y., et al. 2018, *A&A*, **618**, A10
- Deal, M., Goupil, M. J., Marques, J. P., Reese, D. R., & Lebreton, Y. 2020, *A&A*, **633**, A23
- Deal, M., Richard, O., & Vauclair, S. 2021, *A&A*, **646**, A160
- Deheuvels, S., Doğan, G., Goupil, M. J., et al. 2014, *A&A*, **564**, A27
- Denissenkov, P. A. 2010, *ApJ*, **723**, 563
- Dent, T., Stern, S., & Wetterich, C. 2007, *Phys. Rev. D*, **76**, 063513
- Dumont, T., Palacios, A., Charbonnel, C., et al. 2021, *A&A*, **646**, A48
- EGgenberger, P., Maeder, A., & Meynet, G. 2005, *A&A*, **440**, L9
- Ferreira, M. C., Juliao, M. D., Martins, C. J. A. P., & Monteiro, A. M. R. V. L. 2012, *Phys. Rev. D*, **86**, 125025
- Fields, B. D. 2011, *Ann. Rev. Nucl. Part. Sci.*, **61**, 47
- Flambaum, V. V., & Wiringa, R. B. 2007, *Phys. Rev. C*, **76**, 054002
- Fu, X., Bressan, A., Molaro, P., & Marigo, P. 2015, *MNRAS*, **452**, 3256
- García, R. A., Turck-Chièze, S., Jiménez-Reyes, S. J., et al. 2007, *Science*, **316**, 1591
- Gruyters, P., Korn, A. J., Richard, O., et al. 2013, *A&A*, **555**, A31
- Gruyters, P., Lind, K., Richard, O., et al. 2016, *A&A*, **589**, A61
- Iglesias, C. A., & Rogers, F. J. 1996, *ApJ*, **464**, 943
- Iliadis, C., & Coc, A. 2020, *ApJ*, **901**, 127
- Imbriani, G., Costantini, H., Formicola, A., et al. 2004, *A&A*, **420**, 625
- Iocco, F., Mangano, G., Miele, G., Pisanti, O., & Serpico, P. D. 2009, *Phys. Rept.*, **472**, 1
- Korn, A. J., Grundahl, F., Richard, O., et al. 2006, *Nature*, **442**, 657
- Korn, A. J., Grundahl, F., Richard, O., et al. 2007, *ApJ*, **671**, 402
- Kosovichev, A. G. 1988, *Sov. Astron. Lett.*, **14**, 145
- Langacker, P., Segre, G., & Strassler, M. J. 2002, *Phys. Lett. B*, **528**, 121
- Ledoux, P. 1947, *ApJ*, **105**, 305
- Liske, J., Bono, G., Cepa, J., et al. 2014, *Top Level Requirements For ELTHIRES*, Tech. rep., Document ESO 204697 Version 1
- Maeder, A. 2009, *Physics, Formation and Evolution of Rotating Stars*
- Marconi, A., Abreu, M., Adibekyan, V., et al. 2020, *SPIE Conf. Ser.*, **11447**, 1144726
- Marques, J. P., Goupil, M. J., Lebreton, Y., et al. 2013, *A&A*, **549**, A74
- Martins, C. J. A. P. 2017, *Rep. Prog. Phys.*, **80**, 126902
- Martins, C. J. A. P. 2021, *A&A*, **646**, A47
- Mathews, G., Kedia, A., Sasankan, N., et al. 2020, *JPS Conf. Proc.*, **31**, 011033
- Mathis, S., Prat, V., Amard, L., et al. 2018, *A&A*, **620**, A22
- Michaud, G., Fontaine, G., & Beaudet, G. 1984, *ApJ*, **282**, 206
- Michaud, G., Alecian, G., & Richer, J. 2015, *Atomic Diffusion in Stars*
- Morel, P., & Lebreton, Y. 2008, *Ap&SS*, **316**, 61
- Mossa, V., Stöckel, K., Cavanna, F., et al. 2020, *Nature*, **587**, 210
- Muller, C. M., Schafer, G., & Wetterich, C. 2004, *Phys. Rev. D*, **70**, 083504
- Nakashima, M., Ichikawa, K., Nagata, R., & Yokoyama, J. 2010, *JCAP*, **1001**, 030
- Olive, K. A., Petitjean, P., Vangioni, E., & Silk, J. 2012, *MNRAS*, **426**, 1427
- Ouazzani, R. M., Marques, J. P., Goupil, M. J., et al. 2019, *A&A*, **626**, A121
- Palacios, A., Talon, S., Charbonnel, C., & Forestini, M. 2003, *A&A*, **399**, 603
- Pisanti, O., Mangano, G., Miele, G., & Mazzella, P. 2021, *JCAP*, **04**, 020
- Pitrou, C., Coc, A., Uzan, J.-P., & Vangioni, E. 2018, *Phys. Rept.*, **754**, 1
- Pitrou, C., Coc, A., Uzan, J.-P., & Vangioni, E. 2021, *MNRAS*, **502**, 2474
- Rajan, A., & Desai, S. 2020, *PTEP*, **2020**, 013C01
- Richard, O., Michaud, G., & Richer, J. 2001, *ApJ*, **558**, 377
- Richard, O., Michaud, G., & Richer, J. 2002, *ApJ*, **580**, 1100
- Richard, O., Michaud, G., & Richer, J. 2005, *ApJ*, **619**, 538
- Rogers, F. J., & Nayfonov, A. 2002, *ApJ*, **576**, 1064
- Ryan, S. G., Beers, T. C., Olive, K. A., Fields, B. D., & Norris, J. E. 2000, *ApJ*, **530**, L57
- Sbordone, L., Bonifacio, P., Caffau, E., et al. 2010, *A&A*, **522**, A26
- Schwarzschild, M. 1958, *Structure and Evolution of the Stars*
- Seaton, M. J. 2005, *MNRAS*, **362**, L1
- Spite, F., & Spite, M. 1982, *A&A*, **115**, 357
- Stancliffe, R. J. 2009, *MNRAS*, **394**, 1051
- Steigman, G. 2007, *Ann. Rev. Nucl. Part. Sci.*, **57**, 463
- Suda, T., Katsuta, Y., Yamada, S., et al. 2008, *PASJ*, **60**, 1159
- Suda, T., Yamada, S., Katsuta, Y., et al. 2011, *MNRAS*, **412**, 843
- Suda, T., Hidaka, J., Aoki, W., et al. 2017, *PASJ*, **69**, 76
- Talon, S. 2008, *Mem. Soc. Astron. It.*, **79**, 569
- Tayar, J., & Pinsonneault, M. H. 2013, *ApJ*, **775**, L1
- Théado, S., Vauclair, S., Alecian, G., & LeBlanc, F. 2009, *ApJ*, **704**, 1262
- Turcotte, S., Richer, J., Michaud, G., Iglesias, C. A., & Rogers, F. J. 1998a, *ApJ*, **504**, 539
- Turcotte, S., Richer, J., & Michaud, G. 1998b, *ApJ*, **504**, 559
- Vauclair, S. 1988, *ApJ*, **335**, 971
- Vauclair, S. 2004, *ApJ*, **605**, 874
- Yamada, S., Suda, T., Komiya, Y., Aoki, W., & Fujimoto, M. Y. 2013, *MNRAS*, **436**, 1362
- Yeh, T.-H., Olive, K. A., & Fields, B. D. 2021, *JCAP*, **03**, 046
- Zahn, J. P. 1991, *A&A*, **252**, 179
- Zyla, P., Barnett, R. M., Beringer, J., et al. 2020, *PTEP*, **2020**, 083C01